Defective Initiation of Glycosaminoglycan Synthesis due to *B3GALT6* Mutations Causes a Pleiotropic Ehlers-Danlos-Syndrome-like Connective Tissue Disorder

Fransiska Malfait,[1,7,*] Ariana Kariminejad,[2,7] Tim Van Damme,[1] Caroline Gauche,[3] Delfien Syx,[1] Faten Merhi-Soussi,[3] Sandrine Gulberti,[3] Sofie Symoens,[1] Suzanne Vanhauwaert,[1] Andy Willaert,[1] Bita Bozorgmehr,[2] Mohamad Hasan Kariminejad,[2] Nazanin Ebrahimiadib,[4] Ingrid Hausser,[5] Ann Huysseune,[6] Sylvie Fournel-Gigleux,[3] and Anne De Paepe[1]

Proteoglycans are important components of cell plasma membranes and extracellular matrices of connective tissues. They consist of glycosaminoglycan chains attached to a core protein via a tetrasaccharide linkage, whereby the addition of the third residue is catalyzed by galactosyltransferase II (β3GalT6), encoded by *B3GALT6*. Homozygosity mapping and candidate gene sequence analysis in three independent families, presenting a severe autosomal-recessive connective tissue disorder characterized by skin fragility, delayed wound healing, joint hyperlaxity and contractures, muscle hypotonia, intellectual disability, and a spondyloepimetaphyseal dysplasia with bone fragility and severe kyphoscoliosis, identified biallelic *B3GALT6* mutations, including homozygous missense mutations in family 1 (c.619G>C [p.Asp207His]) and family 3 (c.649G>A [p.Gly217Ser]) and compound heterozygous mutations in family 2 (c.323_344del [p.Ala108Glyfs*163], c.619G>C [p.Asp207His]). The phenotype overlaps with several recessive Ehlers-Danlos variants and spondyloepimetaphyseal dysplasia with joint hyperlaxity. Affected individuals' fibroblasts exhibited a large decrease in ability to prime glycosaminoglycan synthesis together with impaired glycanation of the small chondroitin/dermatan sulfate proteoglycan decorin, confirming β3GalT6 loss of function. Dermal electron microcopy disclosed abnormalities in collagen fibril organization, in line with the important regulatory role of decorin in this process. A strong reduction in heparan sulfate level was also observed, indicating that β3GalT6 deficiency alters synthesis of both main types of glycosaminoglycans. In vitro wound healing assay revealed a significant delay in fibroblasts from two index individuals, pointing to a role for glycosaminoglycan defect in impaired wound repair in vivo. Our study emphasizes a crucial role for β3GalT6 in multiple major developmental and pathophysiological processes.

Proteoglycans (PGs) rank among the most abundant and structurally complex biomacromolecules. They are found on the surface of all animal cells and are major components of extracellular matrices (ECM), in particular basement membranes. They are involved in many vital functions including cell-cell and cell-matrix interactions, cell proliferation and migration, cytokine and growth factor signaling, and embryonic and postnatal development and are implicated in several pathological processes such as viral infection.[1–4] PGs consist of a variable number of glycosaminoglycan (GAG) side chains attached to a core protein. GAG chains exhibit considerable structural diversity resulting from a complex biosynthetic pathway, a process that is tightly regulated in biological systems, enabling the modified polysaccharide to selectively interact with a variety of ligands in a spatially and temporally controlled manner.[5] The structure of the core protein and the composition of the GAG chains give rise to a great variety of PGs. GAGs are linear polysaccharides, composed of a repeated disaccharide unit consisting of an amino sugar (N-acetylglucosamine [GlcNAc] or N-acetylgalactosamine [GalNAc]) and an uronic acid (glucuronic [GlcA] or iduronic acid [IdoA]). The PG superfamily is subdivided into two major groups depending on the composition of the disaccharide building block consisting of $(GalNAc\text{-}GlcA)_n$ or $(GlcNAc\text{-}GlcA)_n$ to form chondroitin sulfate (CS)/dermatan sulfate (DS) PGs (e.g., decorin, biglycan, and thrombomodulin) and heparan sulfate (HS) PGs (e.g., perlecan, syndecan, and glypican), respectively. Tightly controlled modifications, such as epimerization and sulfation, further increase the structural and functional diversity of GAGs.[6,7]

The synthesis of GAG chains is initiated by the formation of a tetrasaccharide linker region attached to a serine residue of the PG core protein. This so-called linkage region is indispensable prior to the polymerization of either HS or CS/DS chains, and its synthesis consists of a stepwise process that involves the coordinated action of specific glycosyltransferases (see Figure 1 for details). Synthesis of the linkage region starts by the transfer of xylose onto a serine residue of the core protein catalyzed by xylosyltransferases I/II (encoded by *XYLT1* [MIM 608124] and *XYLT2* [MIM 608125]).[8] Subsequently, two galactose residues are added by galactosyltransferase I (β4GalT7, encoded by *B4GALT7* [MIM 604327])[9,10] and galactosyltransferase II (β3GalT6,

[1]Center for Medical Genetics, Ghent University Hospital, De Pintelaan 185, 9000 Gent, Belgium; [2]Kariminejad-Najmabadi Pathology & Genetics Center, 1143 Med. 4th Str. Third Phase, Shahrak Gharb, 14656 Tehran, Iran; [3]UMR 7365 CNRS-Université de Lorraine (Ingénierie Moléculaire et Pharmacologie Articulaire, IMoPA), MolCelTEG Team, Biopôle UL, Faculté de Médecine, 54505 Vandoeuvre-lès-Nancy, France; [4]Eye Research Center, Farabi Eye Hospital, Tehran University of Medical Sciences, 14656 Tehran, Iran; [5]Department of Dermatology, University of Heidelberg, 69120 Heidelberg, Germany; [6]Biology Department, Ghent University, K.L. Ledeganckstraat 35, 9000 Gent, Belgium
[7]These authors contributed equally to this work
*Correspondence: fransiska.malfait@ugent.be
http://dx.doi.org/10.1016/j.ajhg.2013.04.016.

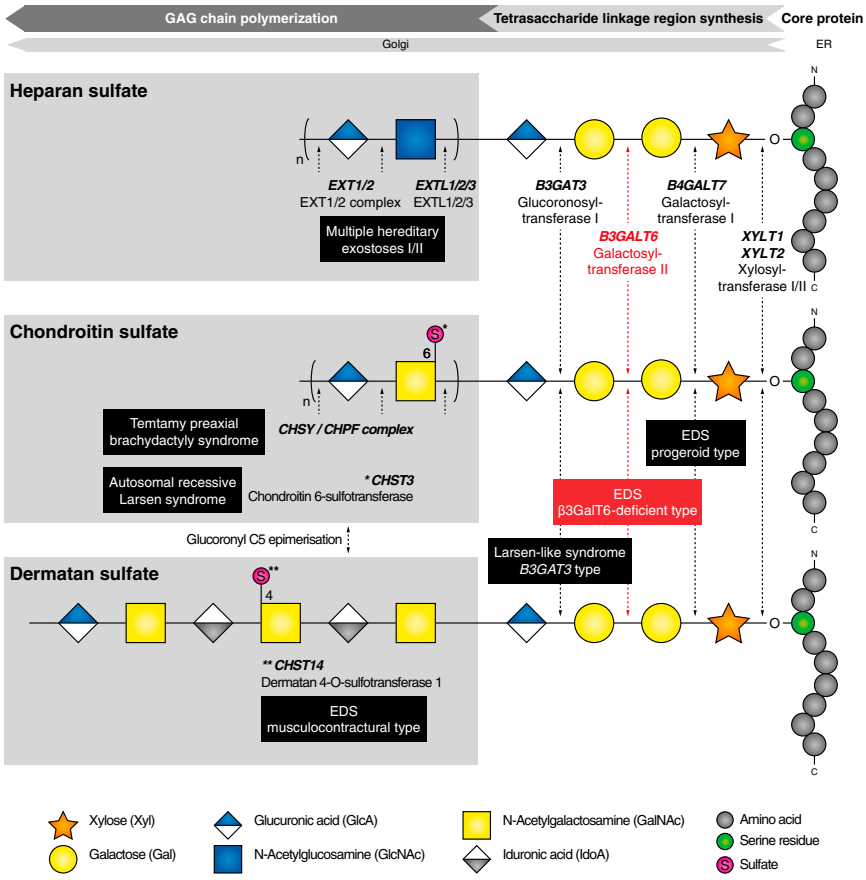

Figure 1. Schematic Illustration of Glycosaminoglycan Synthesis

After synthesis in the endoplasmic reticulum (ER), the core protein is transported to the Golgi apparatus and simultaneously undergoes further modifications. First, a tetrasaccharide linker region is synthesized that originates from the addition of a xylose (Xyl) unit onto a serine residue of the core protein. Subsequent addition of two galactose (Gal) and one glucuronic acid (GlcA) residues completes this process. Depending on the glycosaminoglycan (GAG) chain type, disaccharide units consisting of (N-acetylgalactosamine (GalNAc)-GlcA)$_n$ or (N-acetylglucosamine (GlcNAc)-GlcA)$_n$ are polymerized to form chondroitin sulfate (CS)/dermatan sulfate (DS)-PGs and heparan sulfate (HS)-PGs, respectively. The GAG chain is then further modified by epimerization and sulfation. Genes and the encoded enzymes are indicated in the figure. Disorders resulting from deficiency of the enzymes are indicated in black boxes. The deficient enzyme (β3GalT6) and the related disorder described in the text are depicted in red.

encoded by *B3GALT6*),[11] followed by the transfer of GlcA catalyzed by glucuronosyltransferase I (GlcAT-I, encoded by *B3GAT3* [MIM 606374])[12] to complete the formation of the tetrasaccharide linkage.

The importance of the correct synthesis of GAGs is exemplified by the identification of mutations in genes encoding key enzymes of this synthetic pathway, leading to severe multisystemic disorders in humans. Loss-of-function mutations in *B4GALT7* have been identified in the progeroid form of Ehlers-Danlos syndrome (EDS) (MIM 130070),[13,14] whereas mutations in *B3GAT3* give rise to a Larsen-like syndrome with joint laxity and cardiac defects (MIM 245600).[15] Further down the biosynthetic pathway, mutations in genes involved in the processing of CS, such as *CHST3* (MIM 603799) and *CHSY1* (MIM 608183), are associated with spondyloepiphyseal dysplasia Omani-type (MIM 143095) and recessive Larsen syndrome (MIM 143095)[16] and with Temtamy preaxial brachydactyly syndrome (MIM 605282), respectively.[17] Mutations in *CHST14* (MIM 608429) are associated with musculocontractural EDS (MIM 601776)[18,19] and adducted-thumb-clubfoot syndrome (MIM 601776).[20] Defects in HS synthesis (*EXT1* [MIM 608177] and *EXT2* [MIM 608210]) are linked with hereditary multiple exostoses type I (MIM 133700) and type II (MIM 133701).[21]

Here, we report the identification of mutations in *B3GALT6*, the gene coding for galactosyltransferase II (β3GalT6), in a series of individuals presenting a severe multisystemic disorder, characterized by a unique combination of severe soft connective tissue and bone fragility with multiple early-onset fractures, spondyloepimetaphyseal abnormalities, and intellectual disability. We provide compelling evidence that loss of function of β3GalT6 causes a severe deficiency in GAG synthesis and results in the production of immature decorin, lacking its CS/DS side chain, as well as reduced-to-absent HS chains in dermal fibroblasts of affected individuals. We show that the abnormal PG production perturbs collagen fibril organization and contributes to delayed wound closure.

This study was approved by the Ethics Committee of the Ghent University Hospital (Ghent, Belgium). All affected family members or their legal guardian provided written informed consent.

The index individual P1 (Figures 2A–2D), a 7-year-old child of consanguineous Iranian parents, was born by caesarian section because of breech presentation at 40 weeks of gestation. Birth length, weight, and occipitofrontal circumference (OFC) were 49 cm (50th centile), 3,300 g (50th centile), and 36 cm (36th centile), respectively. She presented with congenital muscle hypotonia and showed mild delay in motor and cognitive development. She was able to hold her head at 4 months and sit at 9 months, said her first words at 18 months, and walked independently at 2 years. Examination at age 7 years revealed a height of 116 cm (50th centile), weight of 18 kg (25th centile), and OFC of 51 cm (50th centile). Facial characteristics included blue sclerae, downslanting palpebral

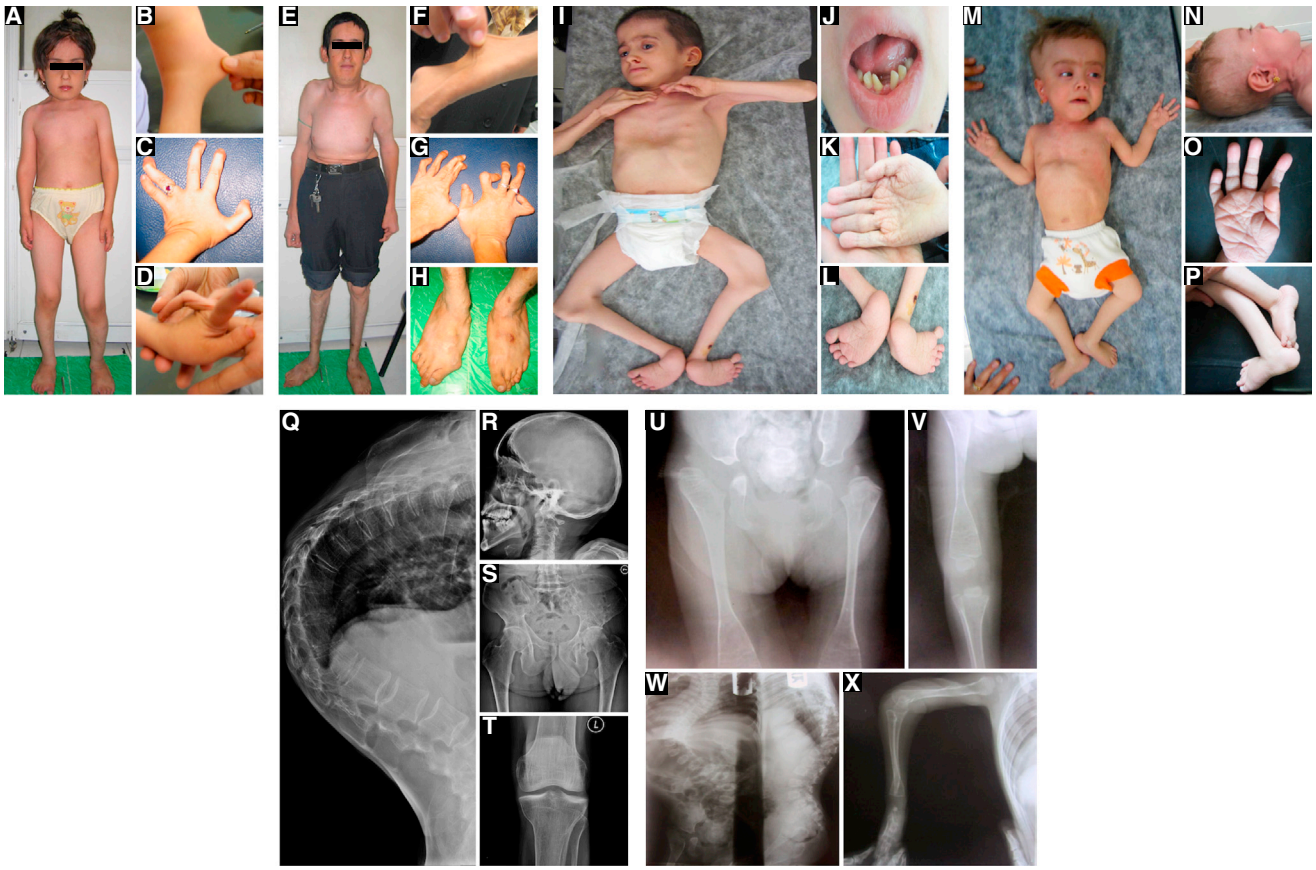

Figure 2. Clinical and Radiological Characteristics
(A–D) P1 at age 7 years, illustrating (A) a hypotonic appearance, bruises on the lower limbs, and broad, flat feet; (B) skin hyperextensibility; and marked hyperlaxity of the finger joints (D) and broad distal phalanges (C).
(E–H) P2 at age 26 years, illustrating (E) disproportionate short stature with short trunk, severe kyphoscoliosis and pectus deformity, and an elongated face with prominent chin; (F) thin and hyperextensible skin; (G) slender, tapered fingers with broad distal phalanges and finger contractures; and (H) broad, flat, and deformed feet and severe hallux valgus.
(I–L) P3 at age 9 years, illustrating (I) severe hypotonia and low muscle mass, short trunk with pectus deformity and kyphoscoliosis, severely deformed lower limbs with contractures and club feet, and mild facial dysmorphism with low-set ears and prognathism; (J) small, yellowish teeth; (K, L) excessive wrinkling of the palms of hand and feet; and (K) spatulate fingers with broad distal phalanges.
(M–P) P5 at age 20 months, illustrating (M) generalized hypotonia, low muscle mass, and pectus deformity; (M, N) a mild progeroid aspect of the face with shallow orbits, blue sclerae, proptosis, short nose, hypoplastic alae nasi, low nasal bridge, sparse hair, and bitemporal narrowing; (O) increased palmar wrinkling and broad distal phalanges; and (P) severe foot deformities.
(Q–T) Radiographs of P2 at age 27 years, illustrating (Q) severe kyphosis, osteoporotic, wedged thoracic vertebral bodies; (R) severe prognathism; (S) flared iliac wings with increased trabecular patterning, coxa valga, and mild degenerative acetabular changes; and (T) osteoporosis of the femur and tibia with increased trabecular patterning.
(U–X) Radiographs of P5 at age 2 years 3 months, illustrating (U) hypoplastic iliac bodies and poorly formed acetabulae; (U, V) osteoporotic aspect of the femur and tibia, diaphyseal narrowing, broadened metaphyses with abnormal trabecular patterning and epiphyseal changes; (W) severe kyphoscoliosis with ovoid vertebrae; and (X) mild bowing of humerus, radius, and ulna.

fissures, low-set ears, thin lips, and early decay of the teeth. She presented a thin, hyperextensible, and transparent skin with visible veins over the thorax. In addition, her skin was fragile, with easy bruising, splitting upon minor trauma, difficult wound closure, and slow wound healing. She presented generalized joint hypermobility and broad, flat feet and had repetitive shoulder dislocations. She had no history of fractures, but bone densitometry performed at age 4 years showed low bone mineral density (BMD) of the spine (L1–L4), with DEXA *Z* score of −2.5 SD. She was treated with intramuscular injection of pamidronate every 3–4 months for 2 years and is currently on oral alendronate. This treatment improved her BMD, as shown by a DEXA *Z* score of L1–L4 of 0.2 SD at age 7 years. She goes to school but is slow in learning. She has mild myopia but no hearing deficit nor cardiac or other internal problems. Pedigree analysis revealed that she has a maternal cousin, individual P2 (Figures 2E–2H), who displayed similar symptoms. This 26-year-old man was born at 40 weeks of gestation after a normal pregnancy and vaginal delivery. Parents were reported unrelated but are from the same geographic region in central Iran. Congenital muscle hypotonia caused delayed gross motor development and inability to sit and walk independently until ages 2 and 7 years, respectively. He has a history of more than 15 atraumatic fractures of the hands and long bones (tibia,

fibula, ulna, and radius) from the age of 7 years. He presented severe generalized joint hyperlaxity in childhood, but progressively developed joint contractures, especially of the finger joints. Kyphoscoliosis was noticed at 7 years of age and progressed over the years. At age 26 years, his height, weight, and head circumference were 146 cm (<3rd centile), 42 kg (<3rd centile), and 51 cm (<3rd centile), respectively. He presented an elongated face with prominent chin, blue sclerae, downslanting palpebral fissures, and small teeth. He had loose, thin, and hyperextensible skin, with splitting upon minor trauma, slow wound healing, atrophic scar formation, and easy bruising. He showed severe kyphoscoliosis, slender fingers with joint contractures and broad distal phalanges, and severe foot deformities with pes planus and hallux valgus. He has mild myopia and mild intellectual disability. Radiographic observations at age 27 years are shown in Figures 2Q–2T.

Both individuals were initially suspected to have EDS VIA (EDS kyphoscoliotic type [MIM 225400]), but the urinary lysylpyridinoline/hydroxylysylpyridinoline (LP/HP) ratio was within normal range, excluding this diagnosis (courtesy of Dr. C. Giunta, University Children's Hospital and Children's Research Center, Zurich). Musculocontractural EDS (EDS type VIB) was excluded by means of molecular analysis of *CHST14*. The parents of P1 were consanguineous, so autosomal-recessive inheritance was assumed and homozygosity mapping was performed in order to identify candidate genes. Both affected persons and seven unaffected family members (Figure 3A) were genotyped with the 200K genome-wide HumanCytoSNP-12 BeadChip SNP array (Illumina). Homozygosity mapping was performed with the web-based HomozygosityMapper application with the recommended default settings, and the results were validated through pairwise genotype clustering with PLINK (v.1.07, default settings).[22,23] This analysis revealed a ~1 Mb homozygous region on chromosome 1 (dbSNP rs3094315 till rs6681938) harboring 63 genes of which 44 encode known or predicted proteins (Figure S1 available online). The coding sequence and 5′ and 3′ untranslated regions (UTRs) of *B3GALT6,* a positional and functional candidate gene, were PCR amplified via gDNA samples from individuals P1 and P2. Amplicons were subsequently analyzed on an ABI 3730XL DNA Analyzer (Life Technologies) with the BigDye Terminator Cycle Sequencing kit (Life Technologies). Comparison with the *B3GALT6* reference sequence (RefSeq accession number NM_080605.3) with the SeqScape Software package (Life Technologies, v.2.5) identified a homozygous missense variant c.619G>C (p.Asp207His) in P1 and P2. The Asp207 amino acid residue (Figure 3B) is highly conserved among species (Figure 3C), and its substitution is predicted to have deleterious effects on protein function (Table S2).

We subsequently studied three additional individuals from two independent families with a similar clinical phenotype. Individual P3 (Figures 2I–2L) is a 9-year-old boy and first child of a nonconsanguineous couple of Iranian origin. The mother is from the same geographic region in central Iran as family 1. He was born at 39 weeks of gestation after an uneventful pregnancy by elective caesarian section with a birth length of 50 cm (50th centile), birth weight of 3,350 g (50th centile), and OFC of 34 cm (50th centile) and presented with clubfeet, congenital bilateral hip dislocation, kyphoscoliosis, and marked muscle hypotonia. He sustained his first fracture at age 12 months during physical examination and since has had multiple fractures after minor trauma. Clinical examination at age 9 years revealed mild dysmorphic features with blue sclerae, low-set ears, small yellowish teeth, asymmetrical skull, and prognathism. He was unable to sit, stand, or walk and spoke only a few words. He had low muscle mass, severe generalized joint hyperlaxity, severe kyphoscoliosis, and pectus excavatum. His skin was loose, hyperextensible, and thin with prominent vessels. He had excessive wrinkling of the dorsum of hands and increased palmoplantar creases on hands and feet, with tapering fingers and broad distal phalanges. At 8 years, a longstanding retinal detachment was detected because of the shrunken appearance of his left eye; deep vitrectomy together with silicone oil injection was performed. Six months later, he needed a revisional surgery as a result of redetachment of the retina. Ophthalmic examination revealed excavation of both optic nerves in the absence of high intraocular pressure in multiple examinations under anesthesia. At 9 years, he sustained a cerebral hemorrhage after a head trauma, for which a craniotomy was performed. His postoperative scar had an atrophic aspect. Echocardiography and evoked auditory brainstem response (EABR) were normal. No radiographs were available.

Individual P4 is the 2-year-old sister of P3. She resides in an institution for disabled children. Although a detailed clinical description on her is not available, it is known that she presents the same phenotype as her brother and a blood sample was obtained. Individual P5 (Figures 2M–2P) is a 20-month-old girl, first and only child of parents from Iranian descent, who are not knowingly consanguineous but originate from the same village in northwestern Iran. She was born after an uneventful pregnancy and delivery at 40 weeks, with a birth length of 47 cm (25th centile), weight of 2,750 g (10th centile), and OFC of 33 cm (25th centile). She showed congenital bilateral hip dislocation and clubfeet. At 4 months of age, she sustained spontaneous bilateral fractures of the femur, and X-rays at the time also revealed an old fracture of the forearm. Subsequently, another fracture of the forearm and rib fractures occurred after minor trauma. Clinical examination at 20 months showed a child with low muscle mass and mild progeroid appearance. Her height was 65 cm (<3rd centile), weight 4,700 g (<3rd centile), and OFC 45 cm (3rd centile). She was unable to hold her head, sit, or stand and had not started to say any words. She had mild dysmorphic features, as illustrated in Figures 2M and 2N. She displayed hyperlaxity of all joints, especially of fingers and wrists. Severe pectus excavatum was

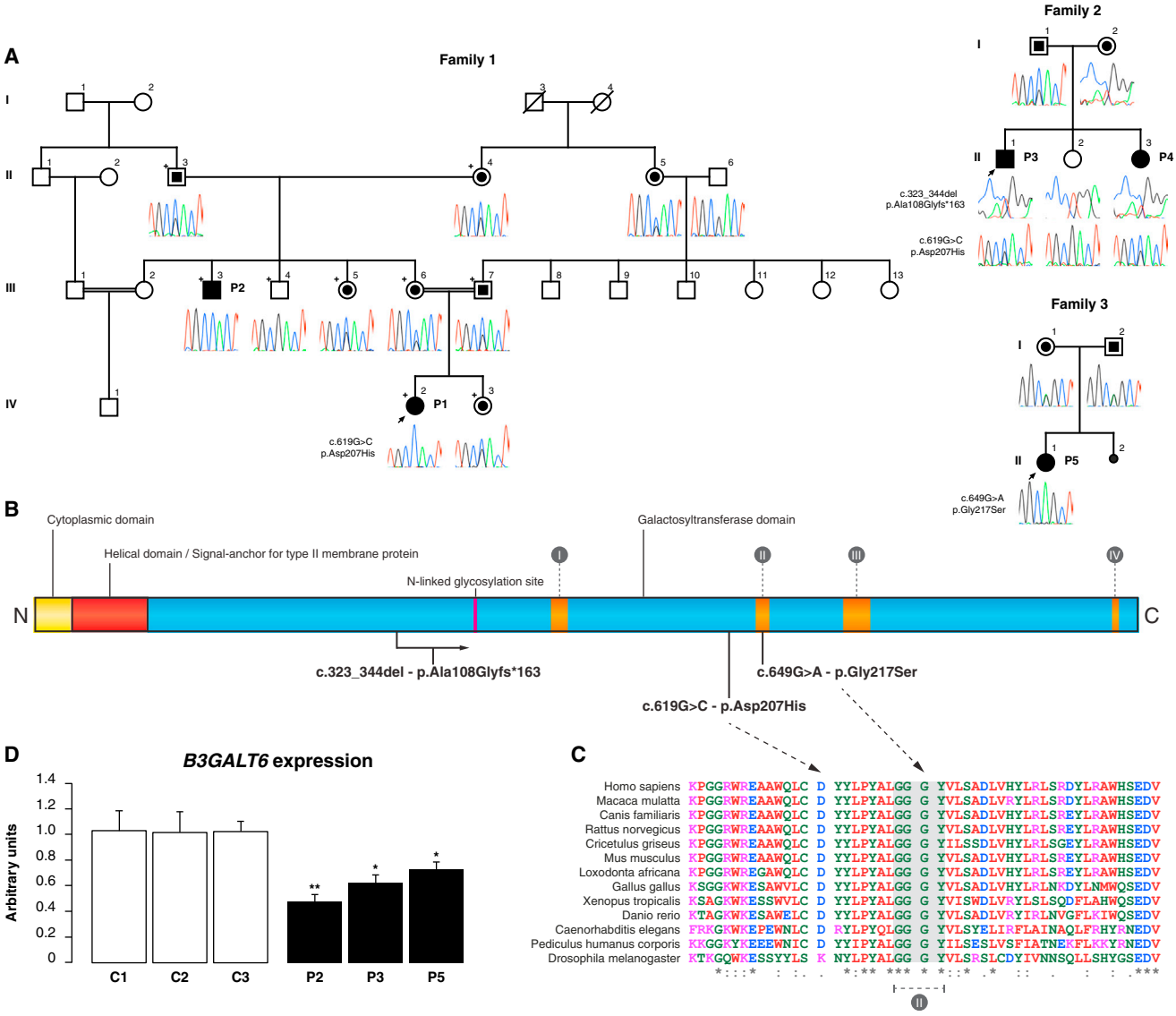

Figure 3. Identification and Analysis of *B3GALT6* Mutations and Their Effect on *B3GALT6* Expression

(A) Pedigrees of families 1–3. Circles indicate females, squares indicate males. Symbols filled in black indicate affected family members with proven homozygous or compound heterozygous *B3GALT6* mutations. Partially filled symbols indicate proven heterozygous carriers. Index persons are indicated by an arrow. Plus sign in the pedigree of family 1 indicates all members included in the homozygosity mapping. Electropherograms are included when available.

(B) Representation of β3GalT6 protein structure with indication of the different domains and positions of the described mutations. Four conserved motifs (I–IV) are shown in orange and a predicted *N*-linked glycosylation site is highlighted in pink.

(C) Clustal Omega protein sequence alignment showing part of the β3GalT6 galactosyltransferase domain including the substituted amino acid residues. The protein sequence is highly conserved across vertebrates, invertebrates, and plants, and Asp207 and Gly217 residues are evolutionary highly conserved (with the latter localized within a consensus motif). Asterisk (*) indicates a single, fully conserved residue; colon (:) indicates strong similar properties (>0.5 in the Gonnet PAM 250 matrix); and period (.) indicates weak similar properties (≤0.5 in the Gonnet PAM 250 matrix). Nucleotide numbering reflects cDNA numbering with +1 corresponding to the A of the ATG translation initiation codon in the reference sequence. At protein level, +1 corresponds to the methionine translator initiator.

(D) qRT-PCR analysis of *B3GALT6* in P2, P3, P5, and three control individuals shows reduced *B3GALT6* expression in affected individuals' samples. Total RNA was extracted with the RNeasy kit (QIAGEN), submitted to DNase Digestion (QIAGEN), and reverse-transcribed with the iScript cDNA Synthesis Kit (Bio-Rad Laboratories). All PCR reactions were carried out in duplicate. Relative expression was determined with the qbase^{PLUS} software (Biogazelle, v.2.4) with *HPRT1* and *YWHAZ* as reference genes. Data are expressed as mean ± SEM; *$p < 0.05$, **$p < 0.01$ (Student's t test).

noted. Her skin was soft and doughy, with increased palmar wrinkling. Radiographic features at age 2 years 3 months are shown in Figures 2U–2X. Sequence analysis of *B3GALT6* in P3 and P4 revealed a 22 bp deletion leading to a frameshift and the introduction of a premature termination codon (c.323_344del [p.Ala108Glyfs*163]) in compound heterozygosity with the c.619G>C (p.Asp207His) mutation. In P5 a homozygous missense mutation

(c.649G>A) resulting in a glycine-to-serine substitution (p.Gly217Ser) was identified. All mutations segregated as expected and were located within the predicted catalytic galactosyltransferase domain of β3GalT6 (Figure 3B). The Gly217 residue is also highly conserved among species (Figure 3C), and its substitution is predicted to have a deleterious effect on protein function (Table S2). Both substitutions were absent in 212 alleles of 106 healthy control individuals and were not described in the 1000 Genomes Project and the NHLBI Exome Sequencing Project (ESP) Exome Variant Server (release ESP6500).

We combined several approaches to assess the functional consequences of *B3GALT6* mutations on β3GalT6 expression and activity, GAG synthesis rate, and CS/DS and HS assembly by using dermal fibroblasts from individuals P2, P3, and P5 and three unrelated healthy controls.

Quantitative RT-PCR (qRT-PCR) experiments revealed significantly reduced *B3GALT6* expression in samples from affected individuals compared to healthy controls (Figure 3D). We next analyzed the effect of the mutations at β3GalT6 protein level and subcellular localization by immunofluorescence microscopy by using anti-β3GalT6 purified MaxPab mouse polyclonal antibody (H00126792-B01P, Abnova) and anti-GOLPH4 rabbit polyclonal antibody (ab28049, Abcam) (Figure S2). In control fibroblasts, β3GalT6 localized to the same subcellular compartment as did GOLPH4, a Golgi-resident protein, confirming previous reports that β3GalT6 is associated with the *cis* Golgi compartment.[11] No apparent modification in the subcellular localization of the protein was observed in affected individuals. However, in fibroblasts of affected individuals, a decrease in β3GalT6 protein level was noticed, as suggested by a reduced staining for β3GalT6 compared to GOLPH4. Together with the reduced transcript level, these data suggest that β3GalT6 is less expressed and/or degraded and that mutations are associated with reduced protein level, in particular in individuals P2 and P3.

To assess the functional consequences of *B3GALT6* mutations on PG-GAG formation, we first analyzed the capacity of control and of P2, P3, and P5 fibroblasts to prime GAG synthesis on the exogenous xyloside 4-methylumbelliferyl-β-D-xylopyranoside (4-MUX, Sigma-Aldrich). The rate of GAG synthesis was evaluated by [$^{35}SO_4$]-incorporation in cultured cells as a function of xyloside concentration, as previously described.[24] Figure 4A shows a strong decrease in the ability of individuals P2 and P5 to prime GAG synthesis compared to the concentration-dependent increase in GAG production in control fibroblasts. In P2 and P5 fibroblasts, GAG synthesis could be detected only at the highest xyloside concentration (10 μM) and reached 55% and 35% that of control fibroblasts, respectively. P3 exhibited a complete lack of priming activity, indicating a profound functional defect in terms of GAG synthesis. In agreement, no detectable in vitro β3GalT6 activity toward the model substrate Gal-Xyl-*O*-methoxynaphthyle could be found in P3 fibroblasts, whereas the activity reached about 10 pmol.min^{-1}.mg protein^{-1} in control fibroblasts (not shown). Next, we examined the synthesis and glycanation of the small CS/DS-PG decorin secreted in affected and control dermal fibroblast cultures by immunoblotting by using an anti-human decorin antibody (Clone 115402, R&D Systems). We observed disturbed processing of decorin in conditioned medium from P3 and P5 fibroblast cultures compared to controls (Figure 4B). In control samples, a single, broad band around 75 kDa corresponding to the GAG-substituted decorin was detected. In P3 and P5 samples, the glycanation of decorin was strongly affected as illustrated by the almost complete loss of GAG substitution in P3 and the presence of a second ~50 kDa band, which was absent in control samples (Figure 4B). Chondroitinase (CSase) ABC digestion showed that this ~50 kDa band corresponds to the unglycanated decorin core protein (Figure S3). Moreover, after CSase ABC digestion, the observed amount of the decorin core protein was significantly lower in the samples from affected individuals as compared to controls. This decrease was more pronounced in P3 than in P5. Concordantly, qRT-PCR showed severely reduced *DCN* expression in fibroblast cultures from affected individuals, compared to controls (Figure 4C). In P3, decreased mRNA levels were also observed for *HSPG2*, encoding perlecan, and *LUM*, encoding lumican. In addition, *XYLT2* and *B4GALT7* expression were also slightly reduced (Figure 4C). To assess whether *B3GALT6* mutations affect HS synthesis as well, we performed immunofluorescence analysis of control and affected dermal fibroblasts by using 10E4 anti-HS monoclonal antibodies, which are commonly used to detect HS chains of cell PGs.[25] Results showed a clear pericellular staining of the HS epitope in control fibroblasts in contrast to a reduced staining intensity in fibroblasts from P2 and P5 and virtually no staining in fibroblasts from P3 (Figure 4D). These data strongly corroborate the idea that *B3GALT6* mutations partially affect HS synthesis in P2 and P5 and result in a virtual loss of HS in P3. Taken together, our data suggest that the *B3GALT6* mutations affect the formation of the linkage region of GAG chains of PGs leading to a defect in both CS/DS and HS-type chain synthesis. The most severe defect was observed in fibroblasts of P3, carrying a compound heterozygous deletion and an Asp-to-His substitution at position 207, leading to reduced *B3GALT6* expression, absence of detectable β3GalT6 activity, and a virtual loss of CS/DS and HS synthesis, whereas fibroblasts from P2 and P5 showed a partial deficiency with reduced β3GalT6 activity, decreased level of GAG synthesis, impaired HS synthesis, and partially CS/DS-substituted decorin.

β3GalT6 belongs to the β1,3-galactosyltransferase family, which exhibits a broad expression in adult human tissues (Figure S4A and Cole et al.[26] and Bai et al.[11]), in line with the multisystemic character of the disorder described in this study. *B3GALT6* is highly conserved among vertebrates, invertebrates, and plants (R. Oriol, S.F.-G., unpublished) and orthologs have been characterized in

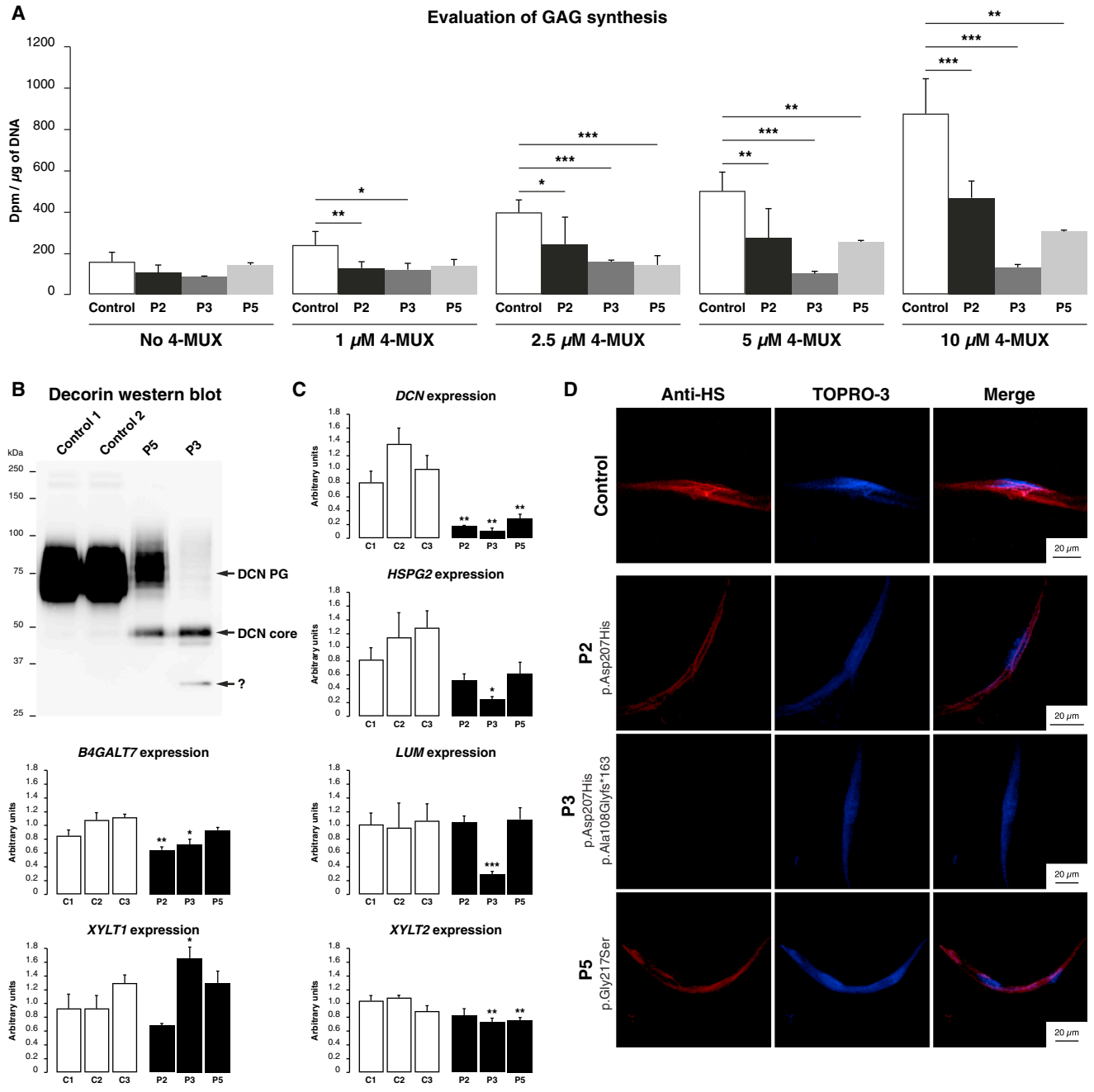

Figure 4. Effect of *B3GALT6* Mutations on β3GalT6 Activity and CS/DS and HS GAG Synthesis

(A) *B3GALT6* mutations affect priming of GAG synthesis. GAG synthesis rate was evaluated in cultured fibroblasts from affected individuals and control by radiolabeled sulfate incorporation from the exogenous xyloside 4-methylumbelliferyl-β-D-xylopyranoside (4-MUX, Sigma-Aldrich) as exogenous substrate as a function of time and concentration.[24] Data are expressed as mean ± SEM; *$p < 0.05$, **$p < 0.01$, ***$p < 0.001$ (Student's t test).

(B) Glycanation of decorin core protein is decreased in P2 and P5 fibroblast cultures compared to controls. Concentrated serum-free conditioned medium was collected at day 7, subjected to SDS-PAGE (4%–12% Bis-Tris gel, Life Technologies) and blotting, and immunolabeled with anti-human decorin antibody (Clone 115402, R&D Systems). The Precision Plus Protein All Blue Standard (Bio-Rad Laboratories) was used as molecular mass marker. Control samples show a broad band of decorin-PG around ~75 kDa. In samples from affected individuals, this decorin-PG band is decreased in intensity, and a second band (~50 kDa) is observed, corresponding to the decorin core protein devoid of its CS/DS chain. In P3 a third, low-molecular band (~32 kDa), possibly a degradation product, is seen.

(C) Confocal immunofluorescence microscopy of HS with 10E4 anti-HS monoclonal antibodies[25] shows a clear pericellular staining of HS epitope in control human fibroblasts, in contrast to a reduced staining intensity for P2 and P5 and virtually no staining for P3 fibroblasts.

(D) qRT-PCR analysis shows a strong reduction of *DCN* expression in all affected persons. A decreased expression of *HSPG2* and *LUM* was observed in P3, whereas slight changes are noted for *XYLT2* and *B4GALT7* in some affected indivuals compared to controls. Experiments were performed in duplicate as described in Figure 3D. Data are expressed as mean ± SEM; *$p < 0.05$, **$p < 0.01$, ***$p < 0.001$ (Student's t test).

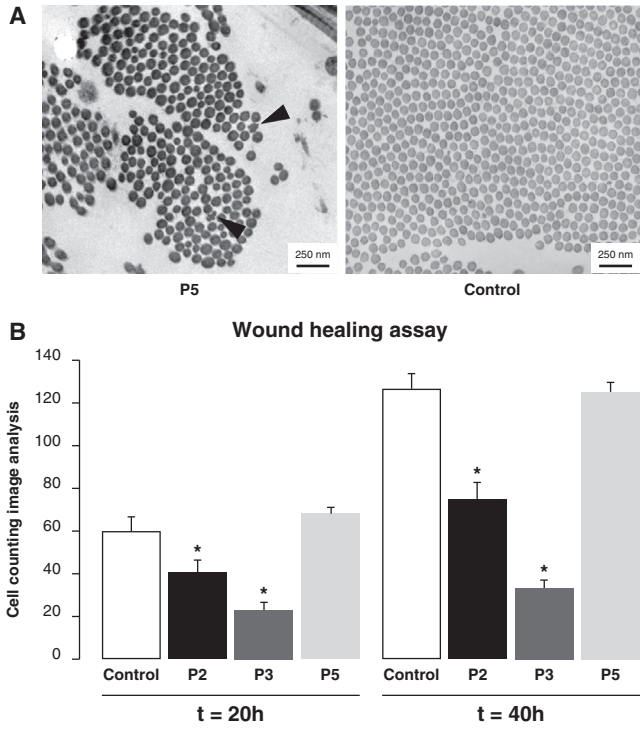

Figure 5. Effect of β3GalT6 Deficiency on Wound Closure and Collagen Fibril and Elastin Ultrastructure

(A) Transmission electron microscopy shows a disturbed collagen organization and ECM architecture. A skin biopsy was taken from the upper anterior thigh of P5, fixed with 3% (w/v) glutaraldehyde in phosphate buffer (pH 7.4), and analyzed with a Zeiss EM900 equipped with a 1K SlowScan CCD camera (Tröndle). The observations were compared with control samples available from the skin biopsy bank of the EM-Lab at Dermatology, University Clinic Heidelberg. Collagen fibrils are loosely packed, with varying fibril diameters and occasional fibrils with very irregular contours (arrowhead).

(B) Quantitative analysis of in vitro wound closure in dermal fibroblasts from β3GalT6-deficient persons shows a delayed wound closure for P2 and P3. Confluent cultures from control, P2, P3, and P5 were subjected to a wound healing assay. Wound closure was monitored 20 and 40 hr after wounding and recorded as number of migrated cells in the denuded area. Data are expressed as mean ± SEM; *$p < 0.05$ (Student's t test).

Drosophila melanogaster[27] and *Caenorhabditis elegans*.[28] The strong conservation of this gene among species is consistent with the key role of β3GalT6 in GAG synthesis and in the control of growth and pattern formation of tissues during development. Interestingly, analysis of the expression profile of *b3galt6* in zebrafish embryos by whole-mount in situ hybridization showed high level of expression in brain, retina, pharyngeal arches, and notochord epithelium, corresponding to tissues that are affected in the deficient persons (Figure S4B). The observation of high β3GalT6 expression in brain at early stages of zebrafish development, together with the presence of intellectual disability in the β3GalT6-deficient individuals, points to an important role of this enzyme in neurogenesis. Indeed, GAG side chains of PGs are increasingly recognized for their critical function in axon guidance and brain development.[29]

β3GalT6 catalyzes the addition of the second galactose residue of the tetrasaccharide linkage of GAG chains, a key step in the initiation of GAG synthesis (Figure 1). Completion of the linker region is prerequisite to the polymerization of both CS/DS and heparin/HS-GAG chains, which are covalently attached to PG core proteins, giving rise to an array of PGs. Our studies provide strong evidence that loss of function of β3GalT6 drastically affects GAG synthesis and assembly. Decorin and biglycan are members of the small leucine-rich PG (SLRP) family, which are important constituents of the interstitial ECM. Decorin is substituted by one GAG chain, mainly of the DS subtype. It plays an important role in the regulation of collagen fibrillogenesis and is essential in maintaining the structural and functional integrity of connective tissues. Indeed, *Dcn*-null mice show severe abnormalities in dermal collagen fiber size and shape and exhibit reduced tensile strength and skin fragility.[30] By transmission electron microscopy on a skin biopsy of P5, we show that β3GalT6 deficiency results in abnormal dermal collagen fibril architecture characterized by loosely packed collagen fibrils of variable size and shape, suggesting that collagen fibrillogenesis is perturbed in this person (Figure 5A). The decorin GAG chain also binds to tenascin-X, another ECM protein involved in regulation of collagen fibril architecture.[31] Symptoms observed in β3GalT6-deficient EDS persons are reminiscent of those observed in tenascin-X-deficient individuals.[32,33] The combination of progressive contractures with striking distal joint hypermobility and muscle hypotonia is also reminiscent of the collagen VI-deficient Bethlem myopathy (MIM 158810) and Ullrich congenital muscular dystrophy (MIM 254090).[34] Type VI collagen is present in most tissues and is enriched close to cells and around basement membranes. It interacts with a broad range of molecules in vitro, including basement membrane components like perlecan and ECM molecules like collagens type I, II, and V, decorin, and biglycan.[35–39] Together, these observations suggest that aberrant CS/DS substitution of SLRPs such as decorin and the resulting defects in collagen supramolecular organization (Figure 5A) are responsible for several of the clinical features observed in the β3GalT6-deficient persons.

As shown in dermal fibroblasts from β3GalT6-deficient persons, *B3GALT6* mutations also produced deleterious effects on HS synthesis, possibly contributing to some phenotypic aspects of the disease, such as defective wound closure. Indeed, it has been reported that cell surface HS-PG of the syndecan family and the secreted matrix HS-PG perlecan modulate wound repair in vivo in a HS-dependent manner.[40–42] Because affected individuals described in this study suffer from impaired wound repair, we employed an in vitro wound healing assay to test whether *B3GALT6* mutations can be linked to this aspect of the phenotype. Compared with control cells, no difference in wound closure was observed in P5. In contrast, in fibroblasts of P2, wound closure was decreased

by about 35% and 40% at 20 and 40 hr time periods, respectively. The delay in wound closure was the most dramatic for P3 (by about 65% and 75% at 20 and 40 hr time period, respectively), in agreement with the severe defect in GAG synthesis that was observed for this person (Figures 5B and S5). These data confirm a role for GAGs in the wound repair process and point to altered GAG function as a possible cause of the delayed wound repair phenotype in the most severely affected β3GalT6-deficient individuals.

The clinical features of the β3GalT6 deficiency phenotype show significant overlap with those of several recessive EDS variants (Table S3). The most significant similarities exist with the musculocontractural and progeroid forms of EDS, conditions that are caused by defects in enzymes that are also involved in GAG synthesis. Distinctive features for β3GalT6-deficient EDS include the progressive nature of the joint contractures, the severe bone fragility with multiple fractures and spondyloepimetaphyseal dysplasia, and the presence of intellectual disability. Clinical overlap also exists with other EDS variants that fall within the EDS type VI spectrum, including EDS type VIA (*PLOD1* [MIM 153454]), spondylocheirodysplastic EDS (MIM 612350, *SLC39A13* [MIM 608735]), and FKBP14-deficient EDS (MIM 614557, *FKBP14* [MIM 614505]). A normal urinary LP/HP ratio allows distinction of β3GalT6-deficient EDS from EDS VIA and spondylocheirodysplastic EDS. The combination of increased palmar wrinkling, progeroid appearance, osteoporosis, and intellectual disability is also reminiscent of recessive cutis laxa variants such as wrinkly skin syndrome (MIM 278250, *ATP6V0A2* [MIM 611716]), geroderma osteodysplasticum (MIM 231070, *GORAB* [MIM 607983]), and De Barsy syndrome (MIM 614438, *PYCR1* [MIM 179035]) (Table S3). Interestingly, the skeletal abnormalities observed in the β3GalT6-deficient EDS persons are highly reminiscent of spondyloepimetaphyseal dysplasia with joint laxity (SEMD-JL) type 1 (MIM 271640), a rare autosomal-recessive skeletal dysplasia first described by Beighton and Kozlowski,[43,44] for which the genetic basis has not yet been established. These observations suggest that β3GalT6-deficient EDS and SEMD-JL are allelic conditions.

In summary, we have shown that mutations in *B3GALT6*, encoding a key enzyme in the formation of the linkage region of the GAG chains of PGs, are responsible for a unique combination of severe generalized symptoms recapitulating Ehlers-Danlos syndrome and characterized by connective tissue fragility, early-onset bone fractures, spondyloepimethaphyseal dysplasia, and intellectual disability. The key role of β3GalT6 in an early step of GAG synthesis and the vital biological functions of PG macromolecules, which range from mechanical support to a variety of extra- and intracellular processes, sustain the idea that mutations in *B3GALT6* underlie a multisystemic disorder that results from disturbances of many physiological processes, including embryonic and postnatal development, maintenance of ECM architecture, and tissue repair.

Supplemental Data

Supplemental Data include five figures and three tables and can be found with this article online at http://www.cell.com/AJHG/.

Acknowledgments

We wish to thank the families for participating in this work. F.M. and D.S. are fellows of the Fund for Scientific Research (FWO), Flanders, Belgium. This work was supported by a Methusalem Grant 08/01M01108 from the Ghent University and Grant G.0171.05 from the Fund for Scientific Research (FWO), Flanders, Belgium, both to A.D.P. This work (C.G., F.M.-S., S.G., S.F.-G.) was funded by Agence Nationale de la Recherche (ANR GAG-Network ANR-08-PCVI-0023), SED66 patient association, Région Lorraine and Université de Lorraine. C.G. is a recipient for a French Ministerial PhD Fellowship. S.F.-G. gratefully acknowledges Mrs. Valérie Gisclard from SED66 for her kind support.

Received: February 19, 2013
Revised: April 11, 2013
Accepted: April 19, 2013
Published: May 9, 2013

Web Resources

The URLs for data presented herein are as follows:

1000 Genomes, http://browser.1000genomes.org
dbSNP, http://www.ncbi.nlm.nih.gov/projects/SNP/
HomozygosityMapper software, http://www.homozygositymapper.org/
MutationTaster, http://www.mutationtaster.org/
NHLBI Exome Sequencing Project (ESP) Exome Variant Server, http://evs.gs.washington.edu/EVS/
Online Mendelian Inheritance in Man (OMIM), http://www.omim.org/
PLINK, http://pngu.mgh.harvard.edu/~purcell/plink/
PolyPhen, www.genetics.bwh.harvard.edu/pph2/
RefSeq, http://www.ncbi.nlm.nih.gov/RefSeq
SIFT, http://sift.bii.a-star.edu.sg/

References

1. Couchman, J.R., and Pataki, C.A. (2012). An introduction to proteoglycans and their localization. J. Histochem. Cytochem. *60*, 885–897.
2. Turnbull, J.E. (2010). Heparan sulfate glycomics: towards systems biology strategies. Biochem. Soc. Trans. *38*, 1356–1360.
3. Bishop, J.R., Schuksz, M., and Esko, J.D. (2007). Heparan sulphate proteoglycans fine-tune mammalian physiology. Nature *446*, 1030–1037.
4. Kreuger, J., Spillmann, D., Li, J.P., and Lindahl, U. (2006). Interactions between heparan sulfate and proteins: the concept of specificity. J. Cell Biol. *174*, 323–327.
5. Prydz, K., and Dalen, K.T. (2000). Synthesis and sorting of proteoglycans. J. Cell Sci. *113*, 193–205.

6. Kusche-Gullberg, M., and Kjellén, L. (2003). Sulfotransferases in glycosaminoglycan biosynthesis. Curr. Opin. Struct. Biol. *13*, 605–611.
7. Bui, C., Ouzzine, M., Talhaoui, I., Sharp, S., Prydz, K., Coughtrie, M.W., and Fournel-Gigleux, S. (2010). Epigenetics: methylation-associated repression of heparan sulfate 3-O-sulfotransferase gene expression contributes to the invasive phenotype of H-EMC-SS chondrosarcoma cells. FASEB J. *24*, 436–450.
8. Götting, C., Kuhn, J., Zahn, R., Brinkmann, T., and Kleesiek, K. (2000). Molecular cloning and expression of human UDP-d-Xylose:proteoglycan core protein beta-d-xylosyltransferase and its first isoform XT-II. J. Mol. Biol. *304*, 517–528.
9. Okajima, T., Yoshida, K., Kondo, T., and Furukawa, K. (1999). Human homolog of *Caenorhabditis elegans sqv-3* gene is galactosyltransferase I involved in the biosynthesis of the glycosaminoglycan-protein linkage region of proteoglycans. J. Biol. Chem. *274*, 22915–22918.
10. Almeida, R., Levery, S.B., Mandel, U., Kresse, H., Schwientek, T., Bennett, E.P., and Clausen, H. (1999). Cloning and expression of a proteoglycan UDP-galactose:beta-xylose beta1,4-galactosyltransferase I. A seventh member of the human beta4-galactosyltransferase gene family. J. Biol. Chem. *274*, 26165–26171.
11. Bai, X., Zhou, D., Brown, J.R., Crawford, B.E., Hennet, T., and Esko, J.D. (2001). Biosynthesis of the linkage region of glycosaminoglycans: cloning and activity of galactosyltransferase II, the sixth member of the beta 1,3-galactosyltransferase family (beta 3GalT6). J. Biol. Chem. *276*, 48189–48195.
12. Kitagawa, H., Tone, Y., Tamura, J., Neumann, K.W., Ogawa, T., Oka, S., Kawasaki, T., and Sugahara, K. (1998). Molecular cloning and expression of glucuronyltransferase I involved in the biosynthesis of the glycosaminoglycan-protein linkage region of proteoglycans. J. Biol. Chem. *273*, 6615–6618.
13. Quentin, E., Gladen, A., Rodén, L., and Kresse, H. (1990). A genetic defect in the biosynthesis of dermatan sulfate proteoglycan: galactosyltransferase I deficiency in fibroblasts from a patient with a progeroid syndrome. Proc. Natl. Acad. Sci. USA *87*, 1342–1346.
14. Bui, C., Talhaoui, I., Chabel, M., Mulliert, G., Coughtrie, M.W., Ouzzine, M., and Fournel-Gigleux, S. (2010). Molecular characterization of β1,4-galactosyltransferase 7 genetic mutations linked to the progeroid form of Ehlers-Danlos syndrome (EDS). FEBS Lett. *584*, 3962–3968.
15. Baasanjav, S., Al-Gazali, L., Hashiguchi, T., Mizumoto, S., Fischer, B., Horn, D., Seelow, D., Ali, B.R., Aziz, S.A., Langer, R., et al. (2011). Faulty initiation of proteoglycan synthesis causes cardiac and joint defects. Am. J. Hum. Genet. *89*, 15–27.
16. Hermanns, P., Unger, S., Rossi, A., Perez-Aytes, A., Cortina, H., Bonafé, L., Boccone, L., Setzu, V., Dutoit, M., Sangiorgi, L., et al. (2008). Congenital joint dislocations caused by carbohydrate sulfotransferase 3 deficiency in recessive Larsen syndrome and humero-spinal dysostosis. Am. J. Hum. Genet. *82*, 1368–1374.
17. Li, Y., Laue, K., Temtamy, S., Aglan, M., Kotan, L.D., Yigit, G., Canan, H., Pawlik, B., Nürnberg, G., Wakeling, E.L., et al. (2010). Temtamy preaxial brachydactyly syndrome is caused by loss-of-function mutations in chondroitin synthase 1, a potential target of BMP signaling. Am. J. Hum. Genet. *87*, 757–767.
18. Miyake, N., Kosho, T., Mizumoto, S., Furuichi, T., Hatamochi, A., Nagashima, Y., Arai, E., Takahashi, K., Kawamura, R., Wakui, K., et al. (2010). Loss-of-function mutations of CHST14 in a new type of Ehlers-Danlos syndrome. Hum. Mutat. *31*, 966–974.
19. Malfait, F., Syx, D., Vlummens, P., Symoens, S., Nampoothiri, S., Hermanns-Lê, T., Van Laer, L., and De Paepe, A. (2010). Musculocontractural Ehlers-Danlos Syndrome (former EDS type VIB) and adducted thumb clubfoot syndrome (ATCS) represent a single clinical entity caused by mutations in the dermatan-4-sulfotransferase 1 encoding CHST14 gene. Hum. Mutat. *31*, 1233–1239.
20. Dündar, M., Müller, T., Zhang, Q., Pan, J., Steinmann, B., Vodopiutz, J., Gruber, R., Sonoda, T., Krabichler, B., Utermann, G., et al. (2009). Loss of dermatan-4-sulfotransferase 1 function results in adducted thumb-clubfoot syndrome. Am. J. Hum. Genet. *85*, 873–882.
21. Duncan, G., McCormick, C., and Tufaro, F. (2001). The link between heparan sulfate and hereditary bone disease: finding a function for the EXT family of putative tumor suppressor proteins. J. Clin. Invest. *108*, 511–516.
22. Seelow, D., Schuelke, M., Hildebrandt, F., and Nurnberg, P. (2009). HomozygosityMapper–an interactive approach to homozygosity mapping. Nucleic Acids Res. *37*, W593–W599.
23. Purcell, S., Neale, B., Todd-Brown, K., Thomas, L., Ferreira, M.A., Bender, D., Maller, J., Sklar, P., de Bakker, P.I., Daly, M.J., and Sham, P.C. (2007). PLINK: a tool set for whole-genome association and population-based linkage analyses. Am. J. Hum. Genet. *81*, 559–575.
24. Talhaoui, I., Bui, C., Oriol, R., Mulliert, G., Gulberti, S., Netter, P., Coughtrie, M.W., Ouzzine, M., and Fournel-Gigleux, S. (2010). Identification of key functional residues in the active site of human beta1,4-galactosyltransferase 7: a major enzyme in the glycosaminoglycan synthesis pathway. J. Biol. Chem. *285*, 37342–37358.
25. van den Born, J., Salmivirta, K., Henttinen, T., Ostman, N., Ishimaru, T., Miyaura, S., Yoshida, K., and Salmivirta, M. (2005). Novel heparan sulfate structures revealed by monoclonal antibodies. J. Biol. Chem. *280*, 20516–20523.
26. Cole, S.E., Mao, M.S., Johnston, S.H., and Vogt, T.F. (2001). Identification, expression analysis, and mapping of B3galt6, a putative galactosyl transferase gene with similarity to *Drosophila brainiac*. Mamm. Genome *12*, 177–179.
27. Ueyama, M., Takemae, H., Ohmae, Y., Yoshida, H., Toyoda, H., Ueda, R., and Nishihara, S. (2008). Functional analysis of proteoglycan galactosyltransferase II RNA interference mutant flies. J. Biol. Chem. *283*, 6076–6084.
28. Hwang, H.Y., Olson, S.K., Brown, J.R., Esko, J.D., and Horvitz, H.R. (2003). The *Caenorhabditis elegans* genes *sqv-2* and *sqv-6*, which are required for vulval morphogenesis, encode glycosaminoglycan galactosyltransferase II and xylosyltransferase. J. Biol. Chem. *278*, 11735–11738.
29. Maeda, N., Ishii, M., Nishimura, K., and Kamimura, K. (2011). Functions of chondroitin sulfate and heparan sulfate in the developing brain. Neurochem. Res. *36*, 1228–1240.
30. Danielson, K.G., Baribault, H., Holmes, D.F., Graham, H., Kadler, K.E., and Iozzo, R.V. (1997). Targeted disruption of decorin leads to abnormal collagen fibril morphology and skin fragility. J. Cell Biol. *136*, 729–743.
31. Mao, J.R., Taylor, G., Dean, W.B., Wagner, D.R., Afzal, V., Lotz, J.C., Rubin, E.M., and Bristow, J. (2002). Tenascin-X deficiency

mimics Ehlers-Danlos syndrome in mice through alteration of collagen deposition. Nat. Genet. *30*, 421–425.
32. Schalkwijk, J., Zweers, M.C., Steijlen, P.M., Dean, W.B., Taylor, G., van Vlijmen, I.M., van Haren, B., Miller, W.L., and Bristow, J. (2001). A recessive form of the Ehlers-Danlos syndrome caused by tenascin-X deficiency. N. Engl. J. Med. *345*, 1167–1175.
33. Voermans, N.C., Jenniskens, G.J., Hamel, B.C., Schalkwijk, J., Guicheney, P., and van Engelen, B.G. (2007). Ehlers-Danlos syndrome due to tenascin-X deficiency: muscle weakness and contractures support overlap with collagen VI myopathies. Am. J. Med. Genet. A. *143A*, 2215–2219.
34. Lampe, A.K., and Bushby, K.M. (2005). Collagen VI related muscle disorders. J. Med. Genet. *42*, 673–685.
35. Tillet, E., Wiedemann, H., Golbik, R., Pan, T.C., Zhang, R.Z., Mann, K., Chu, M.L., and Timpl, R. (1994). Recombinant expression and structural and binding properties of alpha 1(VI) and alpha 2(VI) chains of human collagen type VI. Eur. J. Biochem. *221*, 177–185.
36. Bidanset, D.J., Guidry, C., Rosenberg, L.C., Choi, H.U., Timpl, R., and Hook, M. (1992). Binding of the proteoglycan decorin to collagen type VI. J. Biol. Chem. *267*, 5250–5256.
37. Bonaldo, P., Russo, V., Bucciotti, F., Doliana, R., and Colombatti, A. (1990). Structural and functional features of the alpha 3 chain indicate a bridging role for chicken collagen VI in connective tissues. Biochemistry *29*, 1245–1254.
38. Wiberg, C., Hedbom, E., Khairullina, A., Lamandé, S.R., Oldberg, A., Timpl, R., Mörgelin, M., and Heinegård, D. (2001). Biglycan and decorin bind close to the n-terminal region of the collagen VI triple helix. J. Biol. Chem. *276*, 18947–18952.
39. Symoens, S., Renard, M., Bonod-Bidaud, C., Syx, D., Vaganay, E., Malfait, F., Ricard-Blum, S., Kessler, E., Van Laer, L., Coucke, P., et al. (2011). Identification of binding partners interacting with the α1-N-propeptide of type V collagen. Biochem. J. *433*, 371–381.
40. Stepp, M.A., Gibson, H.E., Gala, P.H., Iglesia, D.D., Pajoohesh-Ganji, A., Pal-Ghosh, S., Brown, M., Aquino, C., Schwartz, A.M., Goldberger, O., et al. (2002). Defects in keratinocyte activation during wound healing in the syndecan-1-deficient mouse. J. Cell Sci. *115*, 4517–4531.
41. Elenius, V., Götte, M., Reizes, O., Elenius, K., and Bernfield, M. (2004). Inhibition by the soluble syndecan-1 ectodomains delays wound repair in mice overexpressing syndecan-1. J. Biol. Chem. *279*, 41928–41935.
42. Zhou, Z., Wang, J., Cao, R., Morita, H., Soininen, R., Chan, K.M., Liu, B., Cao, Y., and Tryggvason, K. (2004). Impaired angiogenesis, delayed wound healing and retarded tumor growth in perlecan heparan sulfate-deficient mice. Cancer Res. *64*, 4699–4702.
43. Beighton, P., Kozlowski, K., Gericke, G., Wallis, G., and Grobler, L. (1983). Spondylo-epimetaphyseal dysplasia with joint laxity and severe, progressive kyphoscoliosis. A potentially lethal dwarfing disorder. S. Afr. Med. J. *64*, 772–775.
44. Beighton, P., and Kozlowski, K. (1980). Spondylo-epi-metaphyseal dysplasia with joint laxity and severe, progressive kyphoscoliosis. Skeletal Radiol. *5*, 205–212.